Geophys. J. Int. (1995) **120**, 237–246

Evidence for a seismic attenuation anomaly beneath the Hida Mountain Range, Central Honshu, Japan

Kei Katsumata, Taku Urabe and Megumi Mizoue

Earthquake Research Institute, The University of Tokyo, Yayoi 1-1-1, Bunkyo-ku, Tokyo 113, Japan

Accepted 1994 May 24. Received 1994 May 24; in original form 1993 July 16

SUMMARY

Previous studies have suggested a low-Q anomaly beneath the Hida Mountain Range (the Japan Alps). However, data have been too sparse to determine propagating characteristics of seismic waves beneath the Japan Alps, or to argue strongly for the existence of the low-Q anomaly.

In order to study the low-Q anomaly in detail, 11 portable seismograph systems were deployed on a line across the northern part of the Japan Alps, Central Honshu, Japan, from July 26 to October 17 in 1989. The seismographs record ground-velocity amplitude. After corrections for the focal mechanisms and site effects by an empirical method, the normalized rms amplitude of P-wave coda was used to study effects of attenuations. It becomes clear in the present study that:

(1) the shallow crust ($z < 3$–5 km) beneath the profile causes normal attenuation of P waves,
(2) strong P-wave attenuation was observed from an intermediate-depth earthquake at some stations close to the crest of the Hida Range, and
(3) a marked low-Q anomaly can be outlined in the crust at 5–15 km depth in the central part of the range, i.e. around Mts Norikuradake, Yakedake and Yarigatake.

The crust at 5–15 km depth beneath these mountains is characterized not only by low Q but also by low velocity, low density and low seismicity. This coincidence suggests the presence of a porous region saturated with a partial melt beneath the Hida Mountain Range.

Key words: attenuation, body wave, Hida Mountain Range, low-Q anomaly, uplift.

1 INTRODUCTION

Seismic waves suffer strong attenuation when propagating in the crust beneath high mountains formed by uplift such as the Himalayan Belt (Ruzaikin, Nersesov & Khalturin 1977) or the Alpine Range (Campillo *et al.* 1993). We will show in this study that a zone of propagation anomaly also exists in the Hida Mountain Range (the Japan Alps), which is the largest mountain range in Japan, located at the triple junction of the Northeastern Japan Arc, the Southwestern Japan Arc and the Izu–Bonin Arc (Fig. 1).

Yamaoka (1981) pointed out that seismic waves which have passed beneath the Japan Alps suffer strong attenuation, which suggests that the Japan Alps may manifest a softened portion of the upper crust that has bulged anelastically under the action of compressive stress. Mizoue *et al.* (1983) found that microearthquakes on the west of the mountain range can hardly be detected by seismic stations deployed on the east of it. Kono *et al.* (1985) reported that S waves passing beneath the Japan Alps at depths between 8 and 20 km attenuate anomalously. Kayano *et al.* (1987) showed that seismic intensities to the west of the range were smaller than those to the east of the range at a similar epicentral distance after the 1986 December 30 magnitude 5.9 earthquake which occurred to the east. They sent inhabitants questionnaires, asking how things moved or shook in the earthquake, and, based on their answers, estimated the seismic intensity, which is defined by the Japan Meteorological Agency (JMA).

These studies were based on data from seismic stations sparsely deployed around the range. If seismic stations are set in a straight array as in an experiment of explosion seismology, it is possible to trace the change of amplitudes along the profile and to construct a model of attenuation beneath the Japan Alps. Direct measurements of absolute amplitude must be corrected for the focal mechanism and

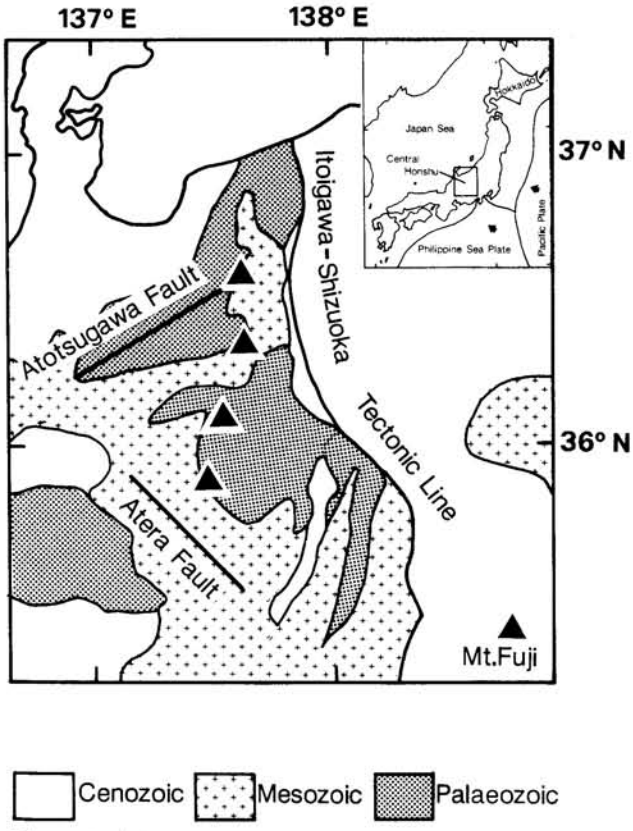

Figure 1. Schematic geological map in and around the Hida Mountain Range. Closed triangles except Mt Fuji represent the mountains in the Hida Mountain Range, Central Honshu, Japan. Bold lines represent main active faults and a tectonic line.

recorder-site amplification before inferences about attenuation can be made. However, except for Kono *et al.* (1985), the effects of focal mechanisms were ignored, and no author corrected for the site effect. Therefore, arguments for low-Q anomaly beneath the Japan Alps have been weak. In this study, we observe seismic waves along a simple straight profile and we consider the effects of focal mechanisms and site amplification when we analysed the data of amplitudes.

2 GEOLOGICAL SETTING

The Japan Alps are the largest mountain range in Japan, located at the triple junction of the Northeastern Japan Arc, the Southwestern Japan Arc and the Izu-Bonin Arc (Fig. 1). The length of the Japan Alps is approximately 150 km and includes mountains up to 3000 m high. Mt Okuhotakadake is 3190 m high, and is the highest peak in the range. The mountain system consists of Palaeozoic to Mesozoic formations. The uplift started at the late Tertiary and continued through the Quaternary. The uplifting rate during the late Quaternary is 1–5 mm yr^{-1}, which is the highest rate known in Japan (National Research Center for Disaster Prevention 1969, 1973). Some Quaternary volcanoes are located in the range, i.e. Mts Tateyama, Yakedake, Norikuradake and Ontake. The mountain systems are bounded by the Itoigawa–Shizuoka tectonic line to the east, which is a huge fault at the western periphery of the Fossa Magna. The Fossa Magna divides Honshu Island geologically into north-east Honshu and south-west Honshu.

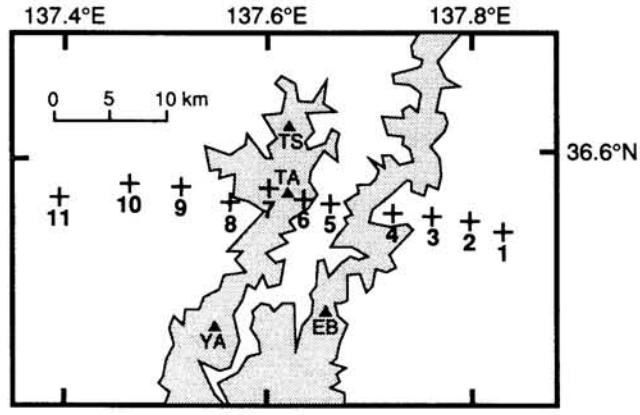

Figure 2. Distribution of seismic stations for temporary observation, from 1989 July 26 to 1989 October 17. Crosses accompanied with numbers, which correspond to numbers in Table 1, show temporary stations. Any other stationary stations are deployed out of this map. Solid lines are contours of 2000 m. Closed triangles are mountain peaks; TS: Mt Tsurugidake; TA: Mt Takyama; EB: Mt Eboshidake; YA: Mt Yarigatake.

3 DATA

Eleven portable seismographs were deployed in a straight array from 1989 July 26 to 1989 October 17, along the Tateyama–Kurobe Alpine Route (Fig. 2 and Table 1). It was the first observation of earthquakes using such a number of seismic stations on the profile in the range. The purpose of this temporary deployment was to record P and S waves passing through the roots of the Japan Alps in order to locate and quantify a possible low-Q anomaly, which was suggested by Yamaoka (1981), Mizoue *et al.* (1983), Kono *et al.* (1985) and Kayano *et al.* (1987). The altitudes of stations were between 360 m and 2425 m. The length of the array was about 40 km from station no. 01 at the east end of the profile to station no. 11 at the west end of it. Each seismograph system, which is described by Urabe & Ohmi (1985), consisted of a set of two components, i.e. up–down and N–S, 2 Hz seismometers (MARK PRODUCTS, L22-D), a time code generator (TCG), dry batteries and an amplifier. The sensitivity of the geophones used was much the same. Waveforms were continuously recorded in direct

Table 1. Location of the temporary seismic stations deployed.

Code	Name	Latitude [° N]	Longitude [° E]	Height [m]
1	Kogumayama	36.5371	137.8323	1079
2	Genyu	36.5481	137.7929	1000
3	Shirasawa	36.5510	137.7601	1110
4	Ogisawa	36.5569	137.7201	1510
5	Kurobeko	36.5592	137.6593	1460
6	Raiden	36.5643	137.6311	2370
7	Murodo	36.5735	137.6001	2425
8	Midagahara	36.5639	137.5615	1955
9	Syomyodaki	36.5768	137.5128	985
10	Bizyodaira	36.5795	137.4636	980
11	Hongu	36.5703	137.3959	360

analogue mode on magnetic tapes. A triggered recording system would not have recorded waves which suffer from strong attenuation. The system passband was from 2 to 20 Hz. Magnetic tapes and dry batteries were replaced every 10 days and 20 days, respectively. About 500 earthquakes were recorded.

The analogue data on magnetic tapes were digitized by means of a personal computer PC-9801VX (NEC, 80286CPU) with an A/D board ADX-98H (CANOPUS). The data were then stored on a magneto-optical disk with a capacity of 594 Mbytes, and were resampled to adjust the sampling rate to 150 Hz. The accuracy of time was maintained within 0.05 s by calibrating the TCG with time tones broadcasted on an AM radio every hour by the Japanese Broadcasting Corporation.

As mentioned above, all seismograph systems were produced in accordance with a standard described in Urabe & Ohmi (1985). However, small differences existed in the characteristics of the recorder systems. Thus, the seismographs were calibrated in the following manner. Instead of signals from a geophone, sine waves with a peak-to-peak voltage of 0.1 V and with a frequency of 10 Hz from a function generator were recorded by each recorder system. After A/D conversion and resampling, the rms of amplitudes were calculated for 60 s. This mean value of amplitudes was used to calibrate the recorders. The frequency of the calibration procedure was chosen at 10 Hz to agree with the dominant frequency of recorded local events.

We used hypocentres and local magnitudes determined by the Kamitakara Geophysical Observatory, Kyoto University (KGO), which includes the three stations of Nagoya University, i.e. Takayama (TAK), Yakedake (YKE) and Takane (TKN), and the Earthquake Research Institute, University of Tokyo (ERI). Earthquakes to the west of the Hida Range were located by KGO and those to the east were located by ERI. The crustal structure which is used for the hypocentre location by KGO (Fig. 3) has been taken

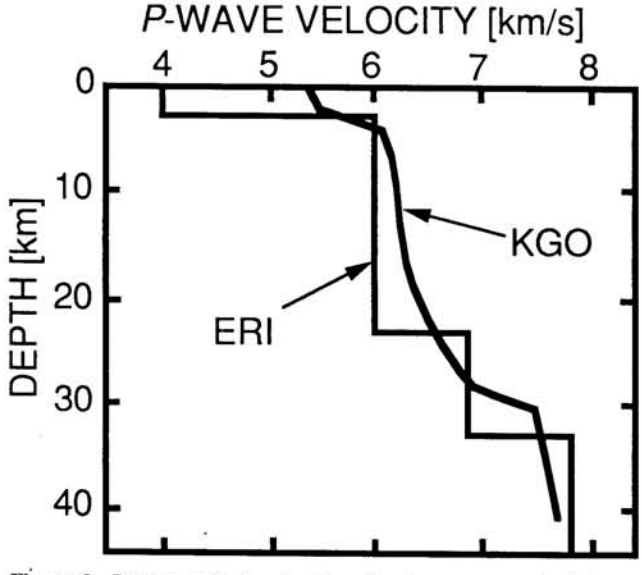

Figure 3. *P*-wave velocity structure for hypocentre calculation at the Kamitakara Geophysical Observatory, Kyoto University (KGO) and Earthquake Research Institute, University of Tokyo (ERI).

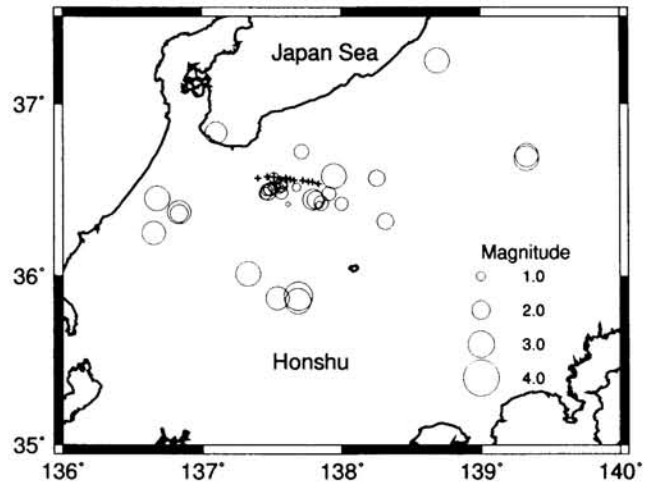

Figure 4. Distribution of epicentres of the 36 local earthquakes which have been used for the estimation of the attenuation factor averaged around the profile. Open circles are epicentres and crosses are the temporary seismic stations.

from three sources (Mikumo 1966; Aoki *et al.* 1972; Wada, Mikumo & Koizumi 1979), and by ERI (Fig. 3), it is based on Hotta *et al.* (1964). The local magnitude is calculated from the duration time both at KGO and ERI.

We chose 36 earthquakes out of 500 as data for the following analysis. The selected earthquakes have various azimuths around the profile to cancel out the azimuthal dependence of 'site effects' (Fig. 4 and Table 2). Local magnitudes ranged from 0.6 to 3.3, and focal depths were shallower than 20 km.

4 METHOD

Two important problems should be taken into account when evaluating anelastic attenuation using amplitudes of seismic waves. First, focal mechanisms affect the amplitudes significantly. Second, local structure at a recording site affects the amplitudes. For example, the amplitudes observed at a station on a thick sedimentary layer can be several times larger than those at a hard-rock site.

4.1 Elimination of the effect of the focal mechanism

The single-scattering model of coda waves elaborated by Aki & Chouet (1975) suggests that *P* coda waves at any given time consist of waves scattered anywhere on the inside wall of an ellipse with two focal points, i.e. a hypocentre and a station. Consider the *P* coda waves which arrive at times T_1 and T_2 at a station. They consist of waves scattered on the walls of two ellipses which bound a volume. Because waves radiated from a source with various emergent angles are superposed, *P* coda waves are less affected by the focal mechanism than the initial *P* waves. Therefore we used the rms of the velocity amplitudes calculated for the portion between T_1 and T_2 as data.

The relation among arrival times of *P* waves T_p, T_1, T_2

Table 2. List of the 36 earthquakes shown in Fig. 4.

No.	Date (y.m.d)	Time (h:m s)	Latitude [°N]	Longitude [°E]	Depth [km]	M
1	1989.07.31	01:09 37.35	36.4534	136.6795	7.1	3.3
2	1989.07.31	20:02 49.80	35.8828	137.6894	3.0	3.8
3	1989.08.02	05:27 18.40	36.5010	137.4640	10.8	1.4
4	1989.08.03	02:07 45.90	36.5431	137.5708	8.6	1.5
5	1989.08.03	02:17 35.93	36.5214	137.5410	3.1	0.8
6	1989.08.06	12:13 18.45	36.5717	138.2550	2.7	2.2
7	1989.08.07	03:55 44.90	37.2497	138.6869	15.5	3.3
8	1989.08.09	19:18 16.23	35.8533	137.6853	3.1	3.4
9	1989.08.10	05:32 38.85	36.7055	139.3361	6.8	3.1
10	1989.08.11	21:40 52.49	36.3674	136.8367	8.8	2.4
11	1989.08.13	01:55 54.53	36.3722	136.8362	9.5	3.1
12	1989.08.22	05:26 47.33	36.5200	137.5170	10.8	1.5
13	1989.08.22	23:52 27.74	35.8700	137.5400	18.2	3.1
14	1989.08.24	01:20 08.42	36.5090	137.4880	5.1	1.7
15	1989.08.24	22:28 52.04	36.3203	138.3161	3.3	2.2
16	1989.08.25	11:45 46.10	36.4160	137.8420	7.7	0.9
17	1989.08.25	16:22 08.70	36.4280	137.8560	1.8	1.9
18	1989.08.26	22:34 44.58	36.5850	137.9470	3.3	3.3
19	1989.08.31	12:57 00.33	36.2518	136.6544	1.0	3.1
20	1989.09.06	07:38 40.80	36.5070	137.4830	9.2	1.6
21	1989.09.06	14:57 02.70	36.4470	137.7970	3.0	2.8
22	1989.09.09	00:47 20.14	36.6866	139.3323	2.2	3.3
23	1989.09.09	15:17 02.60	36.5750	137.5150	13.1	1.3
24	1989.09.09	15:17 08.88	36.5130	137.5540	1.5	1.3
25	1989.09.10	02:44 45.21	36.0132	137.3273	2.0	3.3
26	1989.09.12	10:01 16.18	36.4830	137.4530	5.7	1.6
27	1989.09.13	14:06 55.32	36.4450	137.8160	2.9	2.4
28	1989.09.18	06:19 56.29	36.4800	137.9120	6.6	1.8
29	1989.09.19	03:47 30.40	36.7250	137.7130	20.0	1.9
30	1989.09.21	08:56 28.00	36.4930	137.4730	0.6	2.2
31	1989.09.23	06:24 25.97	36.5240	137.5710	11.0	1.4
32	1989.09.29	05:17 40.39	36.8352	137.0992	9.1	2.9
33	1989.10.01	01:16 20.51	36.4233	138.0017	7.5	1.7
34	1989.10.04	12:03 12.94	36.5190	137.6780	0.5	1.1
35	1989.10.05	15:01 17.32	36.4850	137.5690	0.1	1.6
36	1989.10.10	04:06 47.58	36.4210	137.6170	1.3	0.6

and minor axes of the ellipses are written as,

$$b_1 = \frac{V_p}{2}\sqrt{2\frac{\Delta T_1}{V_p}D + \Delta T_1^2}, \quad (1)$$

$$b_2 = \frac{V_p}{2}\sqrt{2\frac{\Delta T_2}{V_p}D + \Delta T_2^2}, \quad (2)$$

$$\Delta T_1 = T_1 - T_p,$$

$$\Delta T_2 = T_2 - T_p,$$

where D is the hypocentral distance, b_1 and b_2 are minor axes of the inner and the outer ellipses, respectively, and V_p is P-wave velocity. In the analysis, we used 0.3 and 0.8 for ΔT_1 and ΔT_2, respectively. For example, when V_p and D are taken to be 6.0 km s^{-1} and 50 km, respectively, b_1 and b_2 are equal to 7 km and 11 km. When D is 100 km, $b_1 = 10$ km and $b_2 = 16$ km. Thus, using the rms amplitudes of P coda waves rather than the initial P wave reduces the effect of the focal mechanism, but space resolution is limited by the ellipse as estimated in the above examples.

4.2 Elimination of site effects

Site effects were eliminated using the empirical method described below. The amplitudes from earthquakes with various magnitudes were normalized to correspond to earthquakes with a local magnitude of $M = 3.0$ in the following manner. For each earthquake, amplitudes at the 11 stations were plotted against epicentral distance to estimate the constants α_i and β_i in the equation,

$$\log A = \alpha_i - \beta_i \log \Delta, \quad (3)$$

by linear regression. Here A is the velocity amplitude and Δ is the epicentral distance. Then, A_1, which is the amplitude at an epicentral distance of 100 km, is calculated using eq. (3). Next, A_2, which is the amplitude from an earthquake of $M = 3.0$ at an epicentral distance of 100 km, is calculated using eq. (4) (Watanabe 1971),

$$\log A = 0.85M - 5.96. \quad (4)$$

The ratio A_2/A_1 is the magnitude calibration factor for that earthquake. The 11 observed amplitudes were then normalized by this factor to define the calibrated amplitudes. All earthquakes were processed one by one in the same manner. Some 253 calibrated amplitudes were estimated and plotted against epicentral distance. The average attenuation factor for the profile was estimated in terms of the equation,

$$\log A = \alpha_{av} - \beta_{av} \log \Delta, \quad (5)$$

where β_{av} is the average attenuation factor. α_{av} and β_{av} were determined to be 0.052 and 1.5, respectively by linear regression (Fig. 5). If the seismic waves are amplified at the ith station by a site effect, amplitudes observed there would be overestimated, i.e. α_i would be larger than α_{av}. Keeping

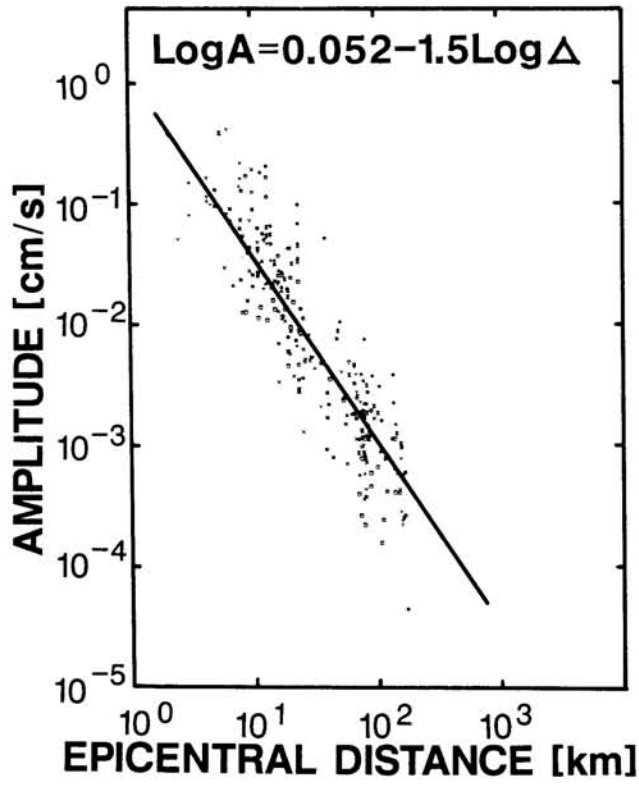

Figure 5. The rms velocity amplitudes versus the epicentral distance. A bold line have been calculated by a least-mean-squares method.

Table 3. Relative station corrections for each station. The negative value of $\alpha_{av} - \alpha$ means that the amplitude observed at a station is amplified by the site effect on the average, and vice versa.

Code	α	$\alpha_{av}-\alpha$
1	0.63	-0.58
2	-0.23	0.28
3	0.07	-0.02
4	0.30	-0.25
5	0.13	-0.08
6	-0.11	0.16
7	0.09	-0.04
8	0.04	0.01
9	0.00	0.05
10	-0.08	0.13
11	-0.14	0.19

β_i fixed as $\beta_i = \beta_{av}$, α_i in eq. (3) was determined by a least-squares method. Then, the corrected amplitude A' at the ith station was defined as

$$\log A' = \log A + (\alpha_{av} - \alpha_i). \quad (6)$$

Table 3 shows the station corrections, i.e. $\alpha_{av} - \alpha_i$, estimated at each station.

5 ATTENUATION BENEATH THE HIDA MOUNTAIN RANGE

After the corrections, the velocity amplitudes of P waves excited by earthquakes which occurred in the upper crust at the east end of the profile, in the upper mantle beneath the profile, and in the southern part of the range were compared event by event.

In the following we present a few examples. First, two cases are shown: an event (1989 August 26, 22:34JST, $M = 3.3$) near station no. 1 at a depth of 3 km (event A in Fig. 6), and an event (1989 August 25, 16:22JST, $M = 1.9$) at a depth of 2 km (event B in Fig. 6). Their waveforms were clearly recorded (see Fig. 7). In both cases, the rms amplitudes decrease almost linearly with epicentral distance (Fig. 8). Anomalous seismic attenuation would manifest itself as the sudden disappearance of waves or sudden decay of amplitudes when waves pass through beneath the Hida

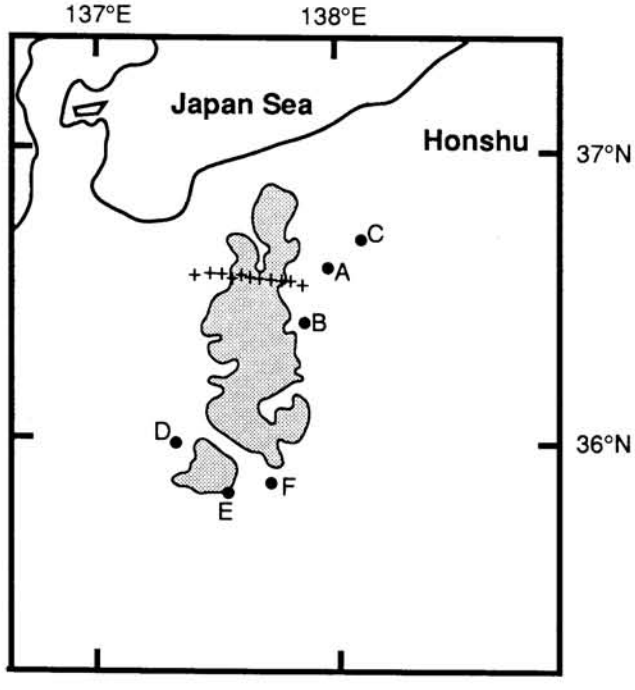

Figure 6. Six (A–F) epicentres which waveforms and amplitudes were presented in this paper are indicated by closed circles. Dotted areas denote the mountain areas higher than 1400 m.

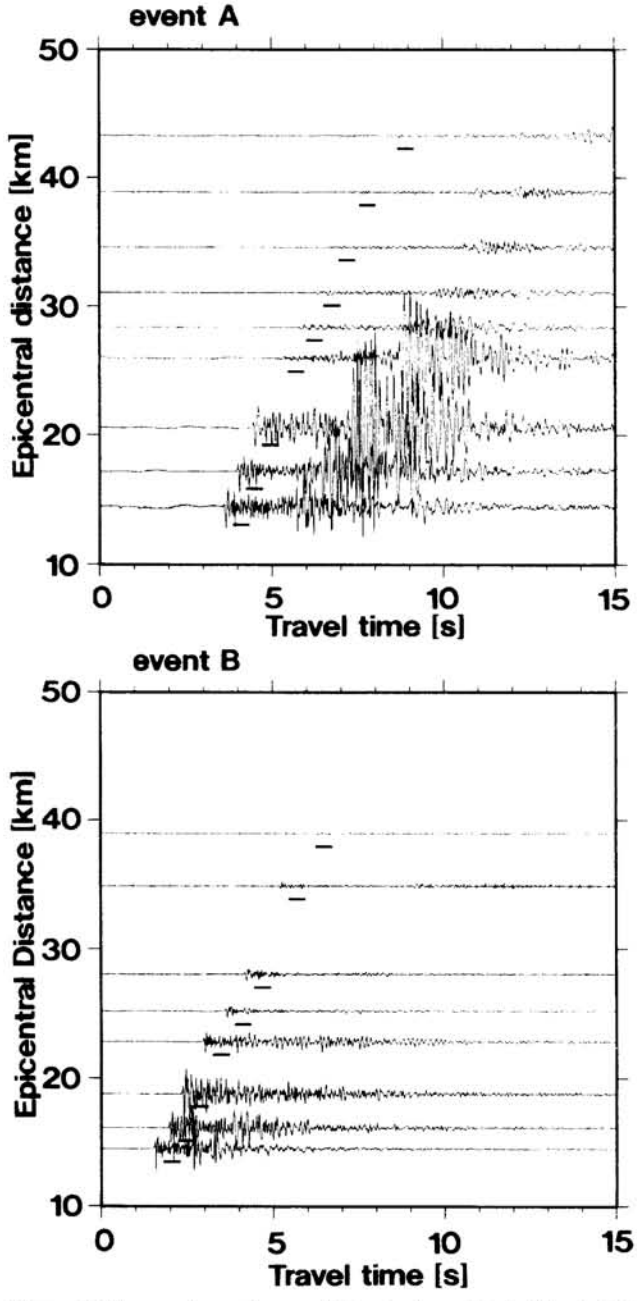

Figure 7. Observed waveforms of Events A and B in Fig. 6. Solid lines with the waveforms indicate the time window for the rms amplitude.

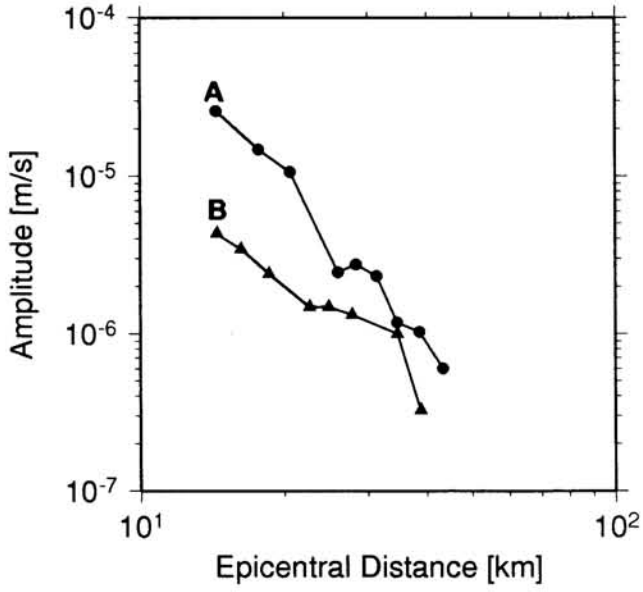

Figure 8. The rms velocity amplitudes versus the epicentral distances for Events A and B in Fig. 6. These are examples of the normal attenuation.

Mountain Range. However, no such effect is seen. Therefore, no anomalous attenuation is recognized just beneath the array. The depth of these ray paths was roughly estimated by ray tracing. As a result, the ray paths went through the crust at depths shallower than 3–5 km beneath the profile.

The amplitudes of an intermediate depth earthquake (1989 October 10, 14:19JST, $M = 3.8$, event C in Fig. 6) at a depth of 207 km are very small at station nos. 5, 6 and 7 with epicentral distances of 45–50 km around the top of the Hida Range (Fig. 9). A very steep decrease is found from 30 to 50 km. Rapid recovery of the amplitude happens between 50 and 70 km. At station nos. 8, 9 and 10, no waveform data could be recorded because of the trouble with the recording system. This phenomenon cannot be explained by geometrical spreading alone. This is evidence for a low-Q anomaly deeper than 3–5 km beneath the profile.

Some ray paths propagating from the south of the profile also attenuate drastically. Three earthquakes are located to the west, the south and the east of the range, respectively, which reveal a pattern of anomalous attenuation which changes as the epicentres move from the west to the east. For the event to the west of the range (1989 September 10, 02:44JST, $M = 3.3$, event D in Fig. 6), the epicentral distance is almost the same for all the stations. The amplitudes at station nos. 1, 2, 3 and 4 are lower by almost an order of magnitude (Fig. 10). For the event to the south of the range (1989 August 22, 23:52JST, $M = 3.1$, event E in Fig. 6), the amplitudes at station nos. 4, 6, 7 and 8 are much smaller than at the other stations (Fig. 11). Except station no. 5, the amplitudes around the top of the range are small. At station no. 11, no waveform data could be recorded because of the trouble with the recording system. From the east (1989 July 31, 20:02JST, $M = 3.8$, event F in Fig. 6), the anomalous attenuation occurs not only at station nos. 4 and 5, but also at station no. 10 on the west side of the Hida

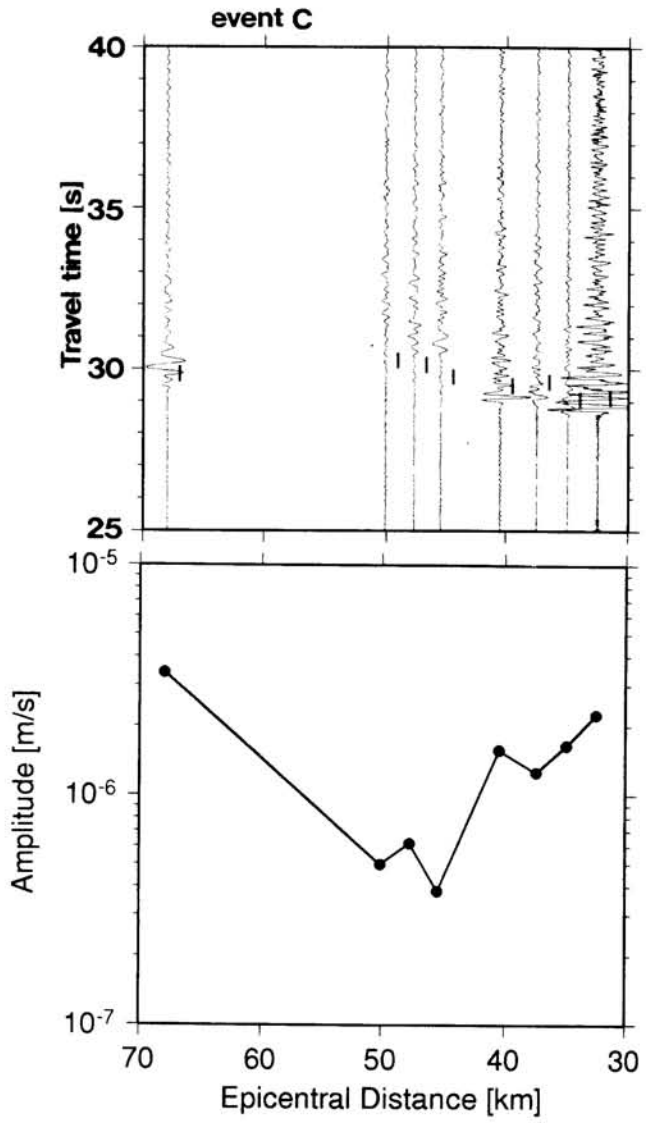

Figure 9. An example of the strong attenuation anomaly. Observed waveforms (above) and the rms velocity amplitudes (below) for Event C in Fig. 6. Solid lines with the waveforms indicate the time window for the rms amplitude.

Mountain Range (Fig. 12). At station nos. 1, 3, 6, 7, 8 and 9, no waveform data could be recorded because of the trouble with the recording system. From these data we conclude that a low-Q anomaly exists around the central part of the Hida Mountain Range (Fig. 13), reaching a depth of 15 km with an upper limit of 3–5 km.

To estimate whether the P-coda waves are affected by the focal mechanism, we determined the focal mechanism, calculated the radiation pattern and compared it with the observed data. The polarity of the first motion of the event shown in Fig. 10 was read at 13 stations (Fig. 14), including our array and observatories of JMA. Note that at station nos. 1, 5 and 6, the first motion is up, and at station nos. 7, 8, 9, 10 and 11, it is down. This fact indicates that one of two nodal planes lies between station nos. 6 and 7. From this focal mechanism, the radiation pattern was calculated (Fig. 10). Apparently the P coda waves are not affected much by

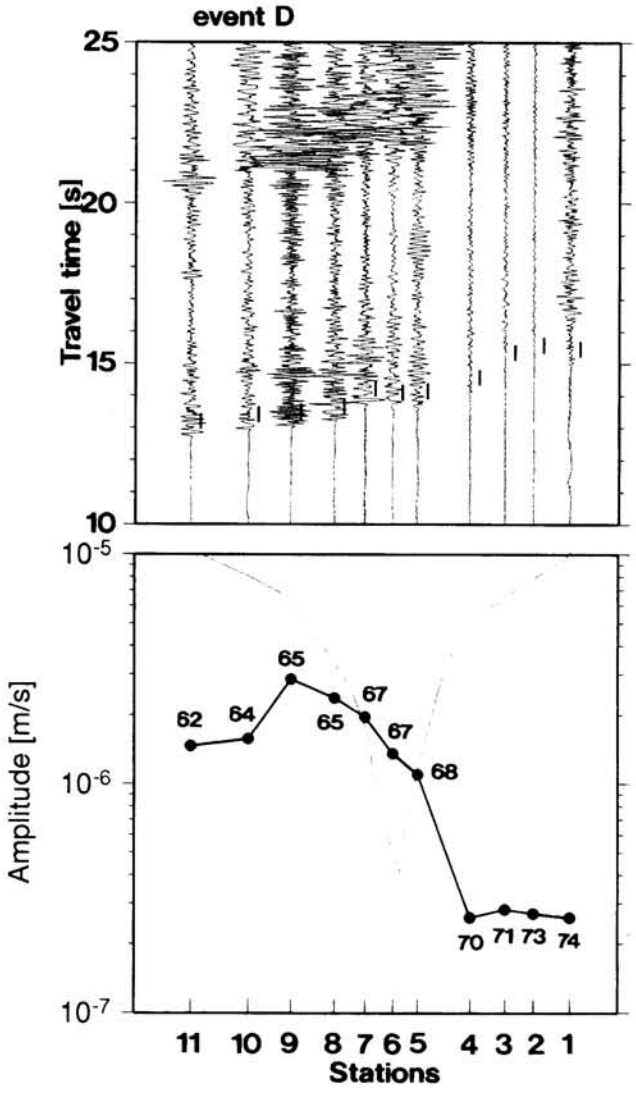

Figure 10. An example of the strong attenuation anomaly. Observed waveforms (above) for Event D in Fig. 6. Solid lines with the waveforms indicate the time window for the rms amplitude. The rms velocity amplitudes at each station (below). Numbers accompanied with closed circles are the epicentral distance in km. A thin solid line indicates a theoretical pattern which is calculated from the focal mechanism shown in Fig. 14. Note that the amplitude at the station no. 11 is supposed to be 10^{-3} cm s^{-1}.

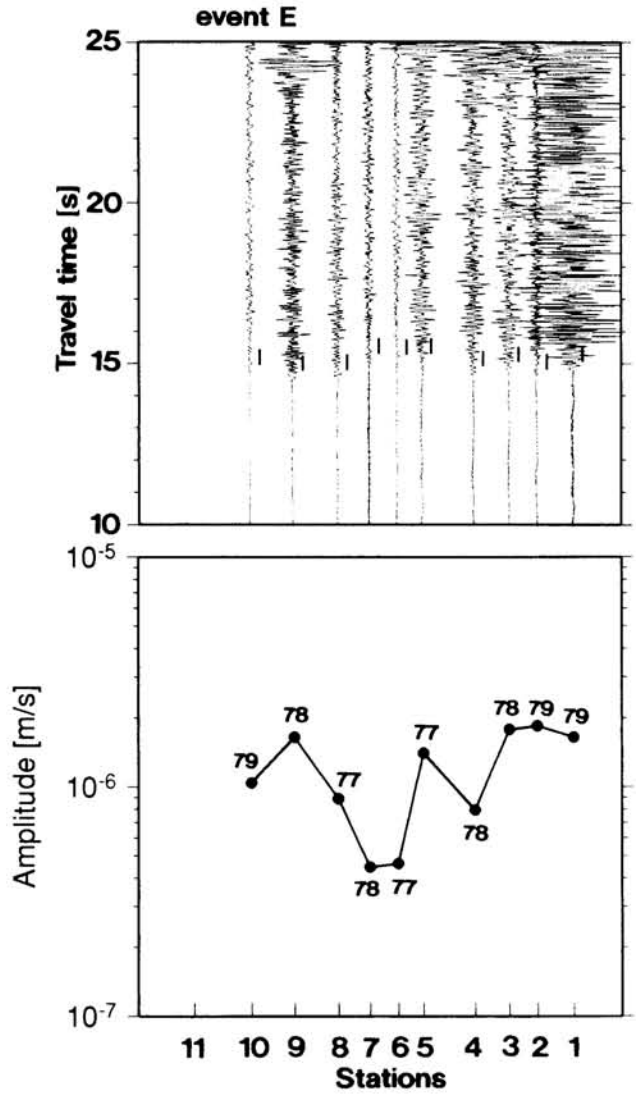

Figure 11. An example of the strong attenuation anomaly (Event E in Fig. 6). Symbols are the same as in Fig. 10.

the focal mechanism. At station nos. 5–11, the drastic change of amplitudes does not appear as the theoretical curve predicts, although the amplitudes at station nos. 9 and 10 were a little larger than those at other stations. Consequently, we are confident that the effect of the focal mechanism on our results is small.

A Q value corresponding to an amplitude reduction of one order can be roughly estimated, assuming the following: P waves with a frequency of 10 Hz and a velocity of 6.0 km s^{-1} propagate, the length of their ray paths is 70 km, and the Q value in the normal crust is 200. Then, the Q value averaged along the ray paths is approximately 100. If the low-Q body is localized in a smaller volume, smaller Q values are needed.

6 DISCUSSION AND CONCLUSIONS

In this study, no low-Q anomaly has been found in the upper crust shallower than 3–5 km just beneath the profile. The data for intermediate-depth earthquakes, however, suggests the existence of a low-Q anomaly which seems to be at a depth of more than 3–5 km. A strong low-Q anomaly has been revealed at a depth of deeper than 5–15 km to the south of our profile, i.e. around Mts Norikuradake, Yakedake and Yarigatake.

Hirahara *et al.* (1989) investigated the 3-D P-wave velocity structure beneath Central Japan in detail by an inversion method. Some 7490 P-wave arrival times from 120 shallow- and intermediate-depth earthquakes that have occurred in this region were used to estimate velocity anomalies in 3-D subdivided blocks and hypocentral perturbations, simultaneously. Although blocks with a size of 0.5° × 0.5° are too large to estimate the small structure in and around the Hida Mountain Range, a low-velocity body exists just beneath Mts Norikuradake, Yakedake and

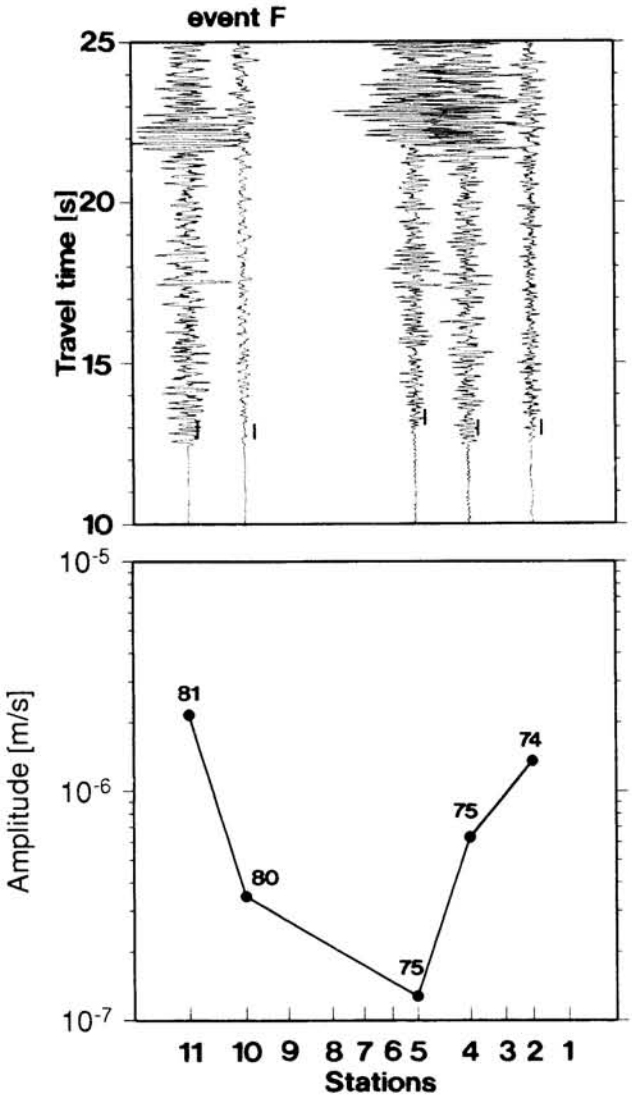

Figure 12. An example of the strong attenuation anomaly (Event F in Fig. 6). Symbols are the same as in Fig. 10.

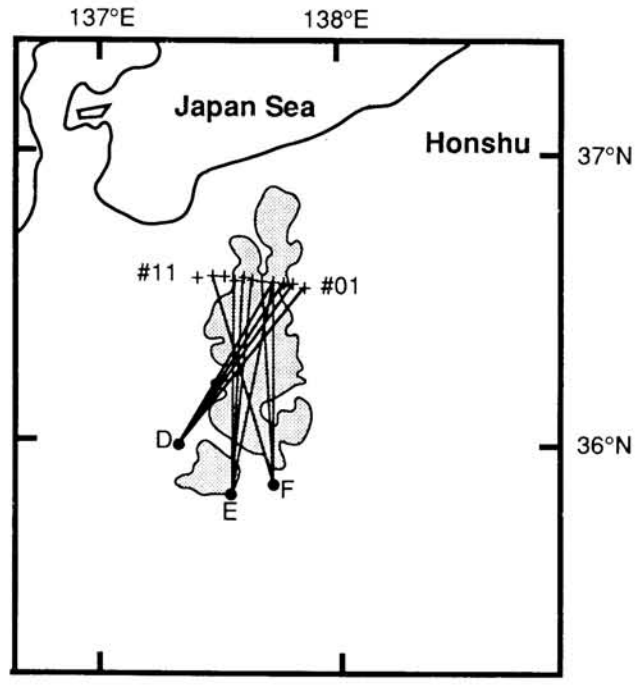

Figure 13. Solid lines indicate couples of the epicentres and the seismic stations where the strong attenuation anomalies were observed.

Yarigatake at a depth of between 0 km and 33 km (Fig. 15). The low-velocity body is spatially correlated with the low-Q zone which we have found in this study.

After Kono & Furuse (1989), the negative Bouguer anomaly in the central part of the Hida Mountain Range is larger than 60 mgal, which is the largest value obtained in Japan (Fig. 16). From these data, Fukao & Yamaoka (1983) interpreted that the anomaly is due to a low-density zone at a depth of between 15 and 25 km, i.e. in the lower crust just beneath the mountains.

High microearthquake seismicity has been observed in an axial portion of the Hida Mountain Range. Mikumo, Wada & Koizumi (1988) have shown the depth distribution of the shocks in the crust in a cross-section parallel to the mountain range. The focal depths of these shocks are shallower than 8 km except in the section of the mountain range to the north of Mt Eboshidake. The maximum focal depth of about 8 km is significantly shallower than in other parts of Central Japan, even if some error of the focal depths is taken into account. This fact implies that the portion deeper than 8 km is ductile because of the high temperature.

This coincidence suggests the presence of a porous region

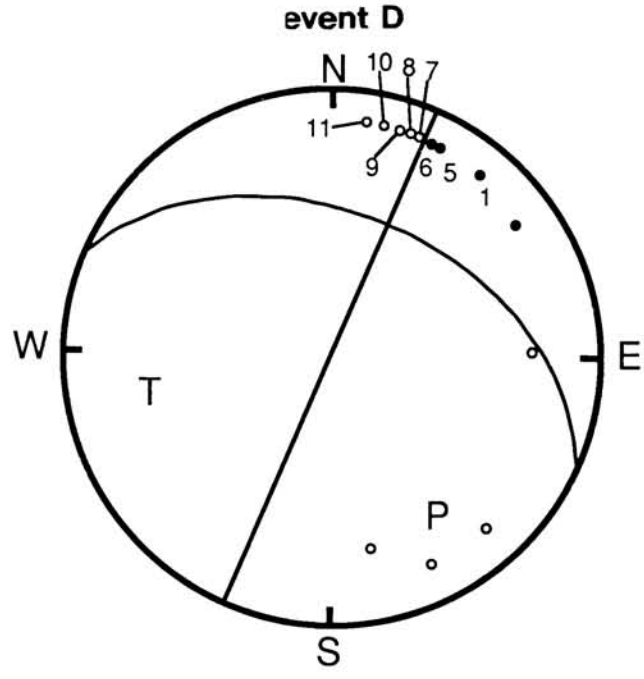

Figure 14. *P*-wave first motions for the shock of 1989 September 10. Diagram is an equal-area projection of the lower hemisphere of the focal sphere. Solid circles represent compressions, open circles dilatations. Circles with station numbers indicate the temporary stations we deployed.

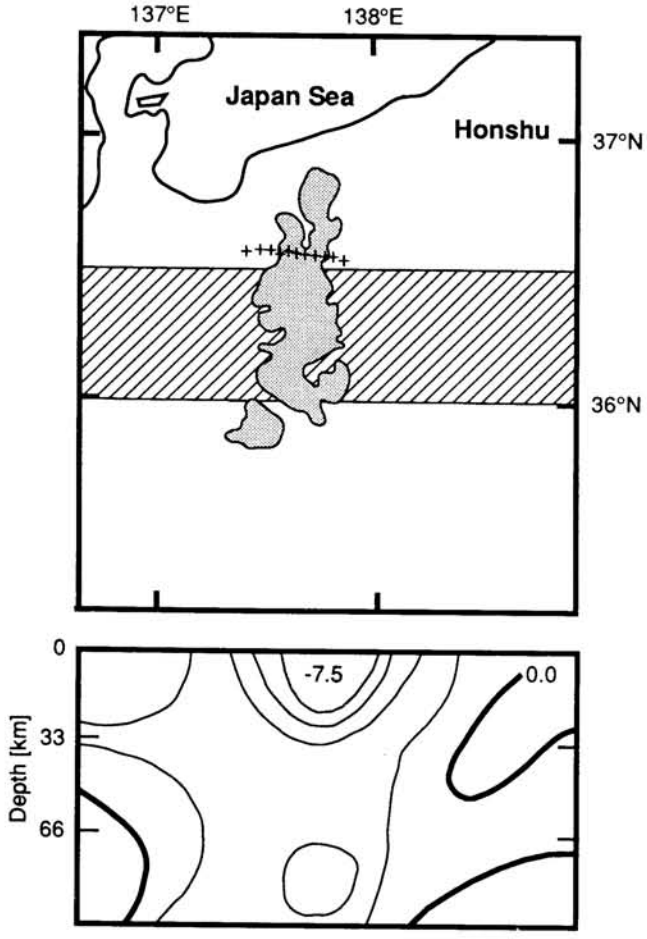

Figure 15. *P*-wave velocity structure beneath the Hida Mountain Range (Hirahara *et al.* 1989). The section (below) corresponds to the shaded area in the map (above). The dotted area in the section indicates the low-velocity body slower than −7.5 per cent.

saturated with partial melts beneath the Hida Mountain Range. A general trend of Q inversely proportional to porosity (Johnston, Toksoz & Timur 1979), and pore fluids act more important role for the attenuation of seismic waves. Shear energy loss simply increases with degree of saturation, and bulk compressional energy loss increases to ~95 per cent saturation (Winkler & Nur 1979). The high temperature causes a decrease in the velocity of seismic waves (Murase & McBirney 1973). Partial melts also contribute to the formation of a low-V zone (Mavko 1980). Since a decrease of density occurs with increasing temperature in some igneous rocks (Murase & McBirney 1973), and the density of a basalt melt is lower than that of its quenched glass at pressures of 0 to 2×10^6 Pa (Fujii & Kushiro 1977, 1978), it is possible to interpret that the low density is caused by the high temperature and resultant partial melts. Moreover, the low seismicity deeper than about 8 km is also consistent with the presence of the partial melting zone.

We emphasize the following three points as conclusions (Fig. 17).

(1) No low-Q anomaly exists in the crust above a depth of 3–5 km just beneath the profile.

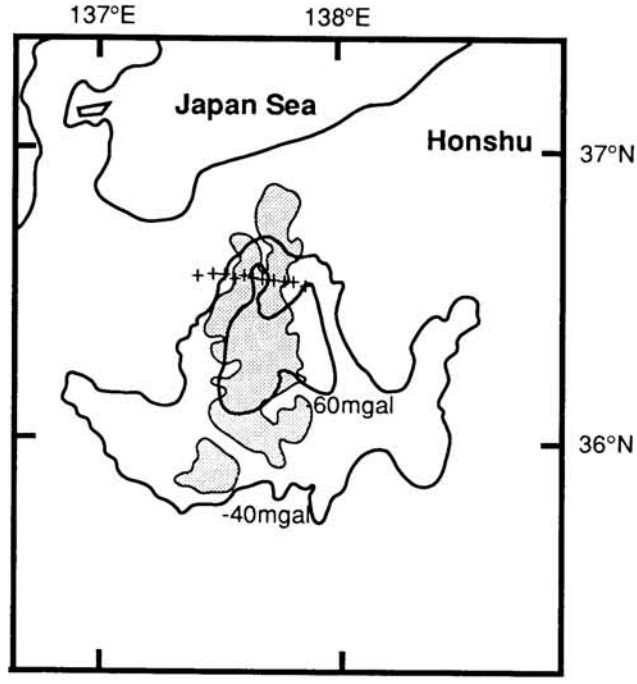

Figure 16. Bouger anomaly of the gravity in and around the Hida Mountain Range (Kono & Furuse 1989). The shaded portion in the map indicates the area where the negative anomaly larger than 60 mgal have been observed. The solid line stands for the contour of −40 mgal.

(2) A strong low-Q anomaly exists at a depth of deeper than 5–15 km to the south of the profile, i.e. around Mts. Norikuradake, Yakedake and Yarigatake.

(3) This low-Q zone beneath the Hida Mountain Range corresponds to the low-velocity zone, the low-density

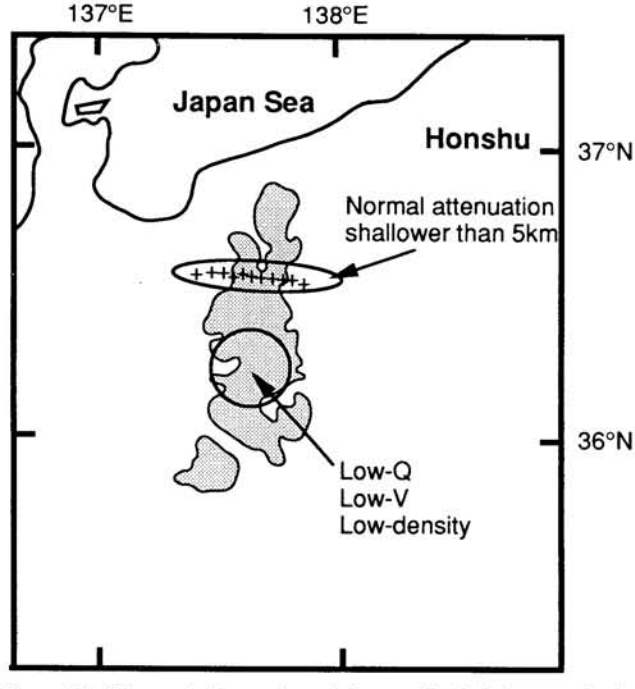

Figure 17. Schematic illustration of the geophysical features in the Hida Mountain Range.

zone and the low-seismicity zone. This coincidence suggests the presence of a porous region saturated with a partial melt beneath the Hida Mountain Range.

ACKNOWLEDGMENTS

We wish to express our hearty gratitude to T. Tsukuda, T. Haneda, S. Hashimoto, K. Sakai and M. Kobayashi for their warmest support of our temporary observations. We are grateful to H. Wada and T. Mikumo in Kyoto University for furnishing valuable data. Discussions with Y. Fukao and S. Kaneshima have been very helpful.

REFERENCES

Aki, K. & Chouet, B., 1975. Origin of coda waves: source, attenuation and scattering effects, *J. geophys. Res.*, **80,** 3322–3342.

Aoki, H., Sasaki, T., Oida, T., Muramatsu, I., Shimamura, H. & Furuya, I., 1972. Crustal structure in the profile across central Japan as derived from explosion seismic observations, *J. Phys. Earth*, **20,** 197–223.

Campillo, M., Feignier, B., Bouchon, M. & Bethoux, N., 1983. Attenuation of crustal waves across the Alpine range, *J. geophys. Res.*, **98,** 1987–1996.

Fujii, T. & Kushiro, I., 1977. Density and viscosity and compressibility of basaltic liquid at high pressures, *Carnegie Inst. Washington, Y. Book*, **76,** 416–424.

Fujii, T. & Kushiro, I., 1978. Density and viscosity of basalt melt at high pressures, GDP—Geodynamics Project (Conference), 1978 March 13–17, Tokyo.

Fukao, Y. & Yamaoka, K., 1983. Stress estimate for the highest mountain system in Japan, *Tectonics*, **2,** 453–471.

Hirahara, K., Ikami, A., Ishida, M. & Mikumo, T., 1989. Three-dimensional *P*-wave velocity structure beneath central Japan: low-velocity bodies in the wedge portion of the upper mantle above high-velocity subducting plates, *Tectonophysics*, **163,** 63–73.

Hotta, H., Murauchi, S., Usami, T., Shima, E., Motoya, Y. & Asanuma, T., 1964. Crustal structure in central Japan along longitudinal line 139E as derived from explosion-seismic observations, *Bull. Earthq. Res. Inst. Univ. Tokyo*, **42,** 533–541.

Johnston, D.H., Toksoz, M.N. & Timur, A., 1979. Attenuation of seismic waves in dry and saturated rocks: II. Mechanisms, *Geophysics*, **44,** 691–711.

Kayano, I., Sakai, K., Kobayashi, M., Haneda, T., Hashimoto, S. & Tsukuda, T., 1987. The letter research of the earthquake occurred at northeastern Nagano prefecture on Des. 30, 1986, *Japanese abstract for the* 1987 *annual meeting of the Seismological Society of Japan*, **2,** 67 (in Japanese).

Kono, Y. & Furuse, N., 1989. 1:1 *million scale gravity anomaly map in and around the Japanese islands*, University of Tokyo Press.

Kono, Y., Kanai, S., Wada, H., Mizoue, M. & Fujii, I., 1985. Anomalous attenuation of seismic waves under the Hida Mountain Range and its cause, 1985, *Japanese abstract for the* 1985 *annual meeting of the Volcanological Society of Japan, Kazan*, **30,** 114 (in Japanese).

Mavko, G. M., 1980. Velocity and attenuation in partially molten rocks, *J. geophys. Res.*, **85,** 5173–5189.

Mikumo, T., 1966. A study on crustal structure in Japan by the use of seismic and gravity data, *Bull. Earthq. Res. Inst.*, **44,** 965–1007.

Mikumo, T., Wada, H. & Koizumi, M., 1988. Seismotectonics of the Hida region, central Honshu, Japan, *Tectonophysics*, **147,** 95–119.

Mizoue, M., Haneda, T., Hashimoto, S., Nakamura, I., Katumata, A. & Yokota, T., 1983. Anomalous seismic wave attenuation beneath the Hida Mountain Range, *Japanese abstract for the 1983 annual meeting of the Seismological Society of Japan*, **2,** 198 (in Japanese).

Murase, T. & McBirney, A. R., 1973. Properties of some common igneous rocks and their melts at high temperatures, *Geol. Soc. Am. Bull.*, **84,** 3563–3592.

National Research Center for Disaster Prevention, 1969. Quaternary tectonic map of Japan, scale 1:2 000 000, Tokyo.

National Research Center for Disaster Prevention, 1973. Explanatory text of the quaternary tectonic map of Japan, Tokyo.

Ruzaikin, A. I., Nersesov, I. L. & Khalturin, V. I., 1977. Propagation of *Lg* and lateral variations in crustal structure in Asia, *J. geophys. Res.*, **82,** 307–316.

Urabe, T. & Ohmi, S., 1985. A small-size, low-cost seismograph system for microearthquake observation using direct analog recording, *Research report of Shimabara earthquake and volcano observatory, Faculty of Science, Kyushu University*, **13,** 27–36 (in Japanese).

Wada, H., Mikumo, K. & Koizumi, M., 1979. Seismicity and focal mechanisms of local earthquakes along the Atotsugawa fault and in the northern Hida Range, *Zisin* (*Bull. seism. Soc. Japan*), **32,** 281–296 (in Japanese with an English abstract).

Watanabe, 1971. Determination of earthquake magnitude at regional distance in and near Japan, *Zisin* (*Bull. seism. Soc. Japan*), **24,** 189–200 (in Japanese with an English abstract).

Winkler, K. & Nur, A., 1979. Pore fluids and seismic attenuation in rocks, *Geophys. Res. Lett.*, **6,** 1–4.

Yamaoka, K., 1981. Focal mechanisms and seismic attenuation in the Hida Mountain Range, Honshu, Japan, *Graduation Thesis*, Nagoya University, Aichi, Japan.